Acta Geotechnica (2016) 11:1075–1085
DOI 10.1007/s11440-015-0420-x

RESEARCH PAPER

# Experimental and numerical investigation into surface strength of mine tailings after biopolymer stabilization

**Rui Chen[1,2] · Xiaobin Ding[1] · Dan Ramey[3] · Ilsu Lee[3] · Lianyang Zhang[1]**

Received: 19 June 2015 / Accepted: 6 October 2015 / Published online: 12 November 2015


**Abstract** Penetration test has been a promising technique for characterizing the surface strength of a crusted surface. This paper presents an experimental and numerical investigation of using a flat-ended penetrometer to evaluate the surface strength of mine tailings (MT) treated with biopolymer solutions of different concentrations. The experimental results show that the infiltration depth of biopolymer solution into dry MT decreases with the increase in biopolymer concentration. Biopolymer stabilization effectively increases the surface strength and cracking resistance of MT, and the increase is greater when the biopolymer concentration is higher. To further explore how biopolymer stabilization increases the surface strength and crack resistance of MT, numerical simulations using discrete element method were carried out to study the penetration tests on MT treated with biopolymer solutions of different concentrations. The simulation results show that the inter-particle tensile and shear strengths both increase with higher biopolymer concentration, indicating that more biopolymer induces larger inter-particle bonding and thus increases the surface strength of MT. The simulation results also confirm the delayed formation of cracks on MT after biopolymer stabilization from a microscale perspective, leading to a better understanding of biopolymer stabilization of MT.

✉ Lianyang Zhang
lyzhang@email.arizona.edu

[1] Department of Civil Engineering and Engineering Mechanics, University of Arizona, Tucson, AZ 85721, USA

[2] School of Highway, Chang'an University, Xi'an 710064, Shanxi, China

[3] Freeport-McMoRan, Oro Valley, AZ 85737, USA

**Keywords** Biopolymer · Discrete element method (DEM) · Dust control · Mine tailings · Penetration test · Surface strength

## 1 Introduction

The mining industry serves to power the growth of economy but leaves a legacy of destructive landscape covered with huge amount of mine tailings (MT). One of the growing environmental concerns related to MT is the wind-borne dust. The dust from MT could be a nuisance to the neighborhoods by reducing visibility along roads, degrading air quality, and contaminating surface water and soil [4]. Besides, the metal-laden particulates within the fugitive dust could be a severe health hazard to human beings [3]. A currently commonly used method to abate the fugitive dust from MT is spraying dust suppressants. A dust suppressant functions in one of the following ways to control dust: retaining moisture within the MT (or soil), transforming smaller particles into larger ones, forming a protective crust at the MT surface, or working as adhesive to bind or agglomerate MT particles together [32]. Recently, the authors have shown that biopolymers are an excellent dust suppressant for mitigating dust from MT without causing negative impact on the environment [8]. Biopolymers can interact with MT particles to form a protective crust at the surface of MT.

It has been well recognized that the crust at MT (or soil) surface plays a crucial role in reducing fine particle entrainment by wind [9, 14, 26]. Even a weak crust can significantly reduce the wind erosion rate [14]. Natural wind-induced shear force seldom directly entrains dust particles from a crusted surface due to the cohesion among the fine particles [9]. It is widely accepted that the saltating particle-induced abrasion and impact disrupt the crust and

generate the dust [9, 13, 26]. During wind erosion, saltating particles repeatedly strike the MT surface inducing disturbance around the impact points. They progressively break the bonding between individual MT particles and disaggregate the crust, exposing the fine particles to wind entrainment and thus increasing wind erosion rate. The erodibility of MT (or soil) depends largely on their mechanical stability, which is defined as the resistance to breakdown by mechanical agents such as wind force, tillage, or abrasion by saltating particles [9]. The mechanical stability derives mainly from the inter-particle bonding of the MT and is closely related to the stress–strain relationship and yield condition of the MT [24].

Rice et al. [28] pointed out that the crust (surface) strength is a good measure to characterize the erodibility of crusted surfaces. Different methods have been proposed to measure the crust strength of soil in order to evaluate its resistance to abrasion by saltating particles. For example, Richards [30] conducted modulus of rupture tests to measure the tensile strength of remolded specimens. However, it is difficult to apply this method in the field. Skidmore and Power [31] proposed an aggregate stability test to measure the crust strength, in which the energy required to crush soil aggregates can be estimated. However, it is difficult to use this method on weak crusts. Previous researches [20, 28, 29] and our study [8] have shown that penetration test is a promising technique for characterizing the surface strength and the surface strength measured by the penetration test shows a good correlation with the dust resistance. For example, Rice et al. [28] studied the erosion of three artificially crusted sediments with varied strength caused by the impact of saltating particles. The strength of each crust was measured using a flat-end cylindrical penetrometer with a diameter of 6 mm prior to wind tunnel test. The flat-ended penetrometer method was preferred to other methods because it applies load to a known area covering many grains and can be easily adapted for use in the field. Their results show that the erosion rate decreases with increasing crust strength measured by the flat-ended penetrometer. Langston and Neuman [20] carried out a series of penetrometer and wind tunnel tests to study the susceptibility of biotic and salt-crusted surfaces to wind erosion. The results show that the crust strength decreases exponentially with increasing number of particle impacts and the penetration test results correlate well with the wind tunnel test results. The authors concluded that the penetrometer test is superior to the portable wind tunnel test because it is easier to perform and less expensive. Therefore, this paper conducts a systematic experimental and numerical investigation on penetration tests of MT in order to better understand how biopolymer stabilization increases the surface strength and the dust resistance of MT.

## 2 DEM simulation of penetration tests

Penetration into soil (or MT) is a large-strain problem involving flow of soil particles and presence of cracks which are difficult to be simulated using continuum theory-based techniques, such as finite difference and finite element methods [15, 25]. Discrete element method (DEM) is a good alternative to solve the large-strain problem, considering that it does not require complex stress–strain laws for the simulated material and fractures are naturally formed at the discrete points, and hence, the nucleation and propagation of the fractures can be investigated without additional effort to reproduce the effect of cracks [11]. DEM has been used to investigate different engineering problems involving large strain such as cone penetration [1, 6, 15], pile penetration [16, 21–23], and soil–tool interaction [25].

Huang and Ma [15] used two-dimensional (2D) DEM combined with boundary-element method (BEM) to explore cone penetration mechanism in sands. The soil near the penetrometer was modeled by an assembly of disks using DEM, and the soil in the far field was simulated using BEM. They found that the soil failure and dilatancy are affected by the loading history. Lobo-Guerrero and Vallejo [22, 23] conducted 2D DEM simulations to investigate the penetration resistance of driven piles in crushable weak sands. The crushable granular particles were simulated by replacing the original particle with an equivalent group of finer particles. When the predefined failure criterion is fulfilled, the particle breaks into a group of smaller ones. The DEM simulation results show that the penetration resistance in the crushable soil is smaller than that in the uncrushable soil. The shape of the driven pile also has a great effect on the penetration resistance and the crushing of the particles. Jiang et al. [16] carried out a numerical study to investigate the deep penetration mechanisms in granular soils using 2D DEM. They found that the tip resistance increases with the penetration depth and the tip-soil friction. The penetration causes the soil near the penetrometer to experience a loading and unloading process, exhibit a complex displacement path, and undergo large rotation of principal stresses.

Simulation of soil penetration problems using 2D DEM is attractive to the researchers, but it may not reflect the real penetration process which is three dimensional (3D) [15]. Few investigations have been performed to simulate the soil penetration problem using 3D DEM. Arroyo et al. [1] performed numerical simulations of cone penetration tests using 3D DEM. The simulated cone resistance showed good agreement with the physical experimental results. Lin and Wu [21] reported a numerical study of driving a penetrometer into granular materials using 3D DEM. It is found that the geometry of the penetrometer has a

significant effect on the tip resistance. Butlanska et al. [6] presented a numerical study of cone penetration tests at micro-, meso-, and macroscale levels using 3D DEM. The numerical results show qualitative agreement with the macroscale observations in the physical tests in sands.

Although DEM has been applied to investigate the penetration into soils, no study has been carried out on using DEM to simulate penetration into MT for evaluating the surface strength. Therefore, this paper uses 3D DEM to simulate the penetration test on MT stabilized with biopolymer solutions of different concentrations, aiming to better understand how biopolymer stabilization increases the surface strength and thus dust resistance of MT.

## 3 Experimental study

### 3.1 Materials

The MT were obtained from a mine site in Southern Arizona and consisted of about 69 % (wt%) of alumina silicate, 30 % quartz, and 1 % pyrite. Figure 1 shows the particle size distribution curve of the MT, indicating that 57.6 % of the MT particles is finer than mesh #100 (150 μm) and 36.4 % is finer than mesh #200 (75 μm). According to ASTM [2], the MT are classified as silty sand.

Xanthan gum was the biopolymer used in this study and was obtained from Gum Technology Corporation in Tucson, Arizona. Xanthan gum was chosen not only because of its low price and well-documented physical and chemical properties, but also because of its capacities to improve the strength of soil and immobilize heavy metals [17, 19].

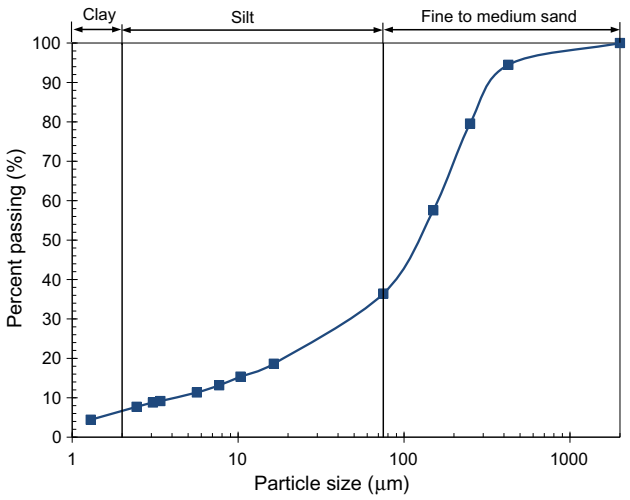


**Fig. 1** Particle-size distribution curve of MT

### 3.2 Specimen preparation

The specimens for penetration tests were prepared using steel trays (22.86 × 22.86 × 5.08 cm). Dry MT were first thoroughly mixed with water at a water content of 25 %. Then, the homogeneous slurry was placed into the steel trays, and each tray contained about 3500 g of wet MT. This process simulates the field operation for pumping the MT slurry into the tailings pond. After the MT in the trays were sun-dried, a sprayer was used to spray biopolymer solution at a concentration of 0 (water only), 0.3, 0.5, or 0.8 %, respectively, on the dry MT surface at an application rate of 1.9 L/m$^2$. The MT specimens treated with water were used as a control. The application rate of 1.9 L/m$^2$ was selected based on the typical application rate from 0.5 to 4.5 L/m$^2$ used in practice [5]. The biopolymer solutions were prepared by dissolving xanthan gum powder in tap water at a specified concentration and stirring the solution for about 10 min until a homogeneous solution was obtained. After spraying the biopolymer solution, all specimens were exposed to sunshine until they were totally dry before tested. For each biopolymer concentration, two specimens were made and tested.

### 3.3 Measurement of infiltration depth of biopolymer solution into dry MT

There are many factors that affect the performance of a dust suppressant in achieving effective dust abatement, including the physical and chemical properties of the dust suppressant, the application rate and frequency of the dust suppressant, the properties of the treated MT (or soil), the environmental conditions, the infiltration depth of the suppressant, and the longevity of the suppressant [10, 18]. Bolander and Yamada [5] suggested that maximum dust control effect can be achieved by ensuring sufficient infiltration depth of the liquid dust suppressant because adequate suppressant infiltration depth helps to resist surface wear, prevent leaching, impart cohesion, and prolong service life. They suggested that the suppressant infiltration depth should be 10–20 mm for road dust control. Copeland et al. [10] also suggested that the suppressant infiltration depth is the most critical factor in achieving effective dust control. Therefore, in this study, the infiltration depth of biopolymer solution into the dry MT was measured. The MT specimens used for measuring the infiltration depth of biopolymer solution were prepared in the same way as those for the penetration tests. After the sun-dried MT specimens were sprayed with biopolymer solutions of different concentrations (0, 0.3, 0.5, and 0.8 %), they were allowed to cure for 30 min and then cut vertically into several pieces with care to measure the infiltration depth of biopolymer solution. The same biopolymer solution

application rate of 1.9 L/m$^2$ as that for the penetration tests was used.

### 3.4 Penetration tests

A flat-ended cylindrical penetrometer with a diameter of 6 mm was manufactured and mounted to an ELE Tri Flex 2 loading machine in order to perform the penetration tests [8]. Figure 2 shows the location and sequence of the penetration tests for each specimen. The first penetration (P1) was at the center, and the rest four were on the diagonals and approximately 6 cm from the center, ensuring a distance of at least ten times the penetrometer diameter between the penetration locations and between a penetration location and the tray edge. To perform the penetration test, the prepared MT specimen tray was placed on the loading platform and the penetrometer was adjusted so that its flat end just touches the MT surface. Then, the penetrometer was driven into the MT specimen at a constant loading rate of 0.1 mm/min, until reaching a total penetration of 4.0 mm. The force and penetration were recorded during the penetration test. Pictures were also taken before and after each penetration test.

## 4 Experimental results

Figure 3 presents the typical pictures showing the infiltration depth of biopolymer solution at a concentration of 0, 0.3, 0.5, and 0.8 %, respectively, into the dry MT specimens 30 min after the spraying. It can be seen that the infiltration of biopolymer solution is not even due to the heterogeneity of the MT. A biopolymer solution at lower concentration shows greater infiltration depth into the dry MT, simply because of its lower viscosity. Based on eight measurements for each biopolymer concentration, the infiltration depths are 21–27, 15–20, 13–17, and 11–15 mm for the biopolymer solution at a concentration of 0, 0.3, 0.5, and 0.8 %, respectively. Fuller and Marsden [12] conducted a study on using guar gum to mitigate dust generation in dry playa areas. They used a biopolymer concentration of 0.9 % and an application rate of 1.9–3.8 L/m$^2$. They found that the infiltration depth was between 4 and 7 mm 30 min after the application of the guar gum solution. The infiltration depth in the current study is larger than that in the study by Fuller and Marsden [12], simply because the xanthan gum solution used in the current study has lower concentration and much lower viscosity than the guar gum solution used in their study.

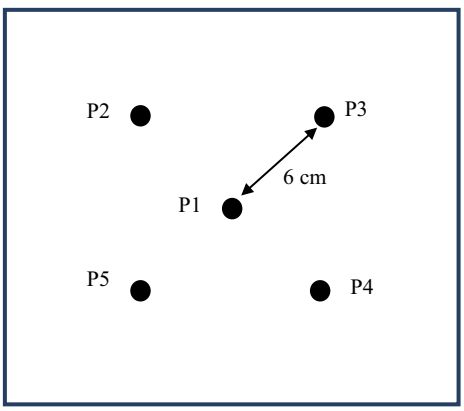


**Fig. 2** Location and sequence of penetration tests

Figure 4 compares the surface condition after each penetration test on the MT specimens treated with 0 (water), 0.3, and 0.8 % biopolymer solutions, respectively. After the first penetration test (P1), a crack is generated on the water (0 %)-treated specimen but not on the 0.3 or 0.8 % specimen. The second penetration test (P2) extends the previously generated crack and generates new cracks coalescing it on the 0 % specimen, but it generates only two small cracks on the 0.3 % specimen or no crack on the 0.8 % specimen. After more penetration tests, new cracks and/or crack coalescences are observed on both the 0 and 0.3 % specimens, with the 0 % specimen showing more cracks than the 0.3 % specimen. However, only a single small crack is observed on the 0.8 % specimen after the fourth penetration test (P4). Figure 4 clearly indicates the increase in cracking resistance (related to tensile strength and thus dust resistance) of MT after biopolymer stabilization, higher biopolymer concentration leading to greater increase in the cracking resistance. Figure 4 also suggests that with the increase in penetrations, which corresponds to the increase of saltation duration in the field, the crust is progressively degraded due to the accumulation of micro-cracks.

Figure 5 shows the typical penetration force versus penetration depth curves from the penetration tests. Curve *a* shows steady increase in penetration force with penetration depth with no drop. This type of curve was generally observed during the first penetration test (P1) on biopolymer-treated specimens, in which the force first increases with penetration up to a certain level and then remains nearly unchanged until the end of the test, suggesting no obvious surface crack (drop of force) or stable crack propagation during the penetration. Curve *b* shows one obvious drop during the penetration, as observed during the first penetration test (P1) on the 0 % specimen or the second (P2) and/or third (P3) penetration test on the 0.3 and 0.5 % specimens, indicating the formation of one crack. After several penetration tests, the force–penetration curves may show multiple drops, as observed during the fourth (P4) and/or fifth (P5) penetration test on the 0, 0.3, and 0.5 % specimens (Curve *c*). This

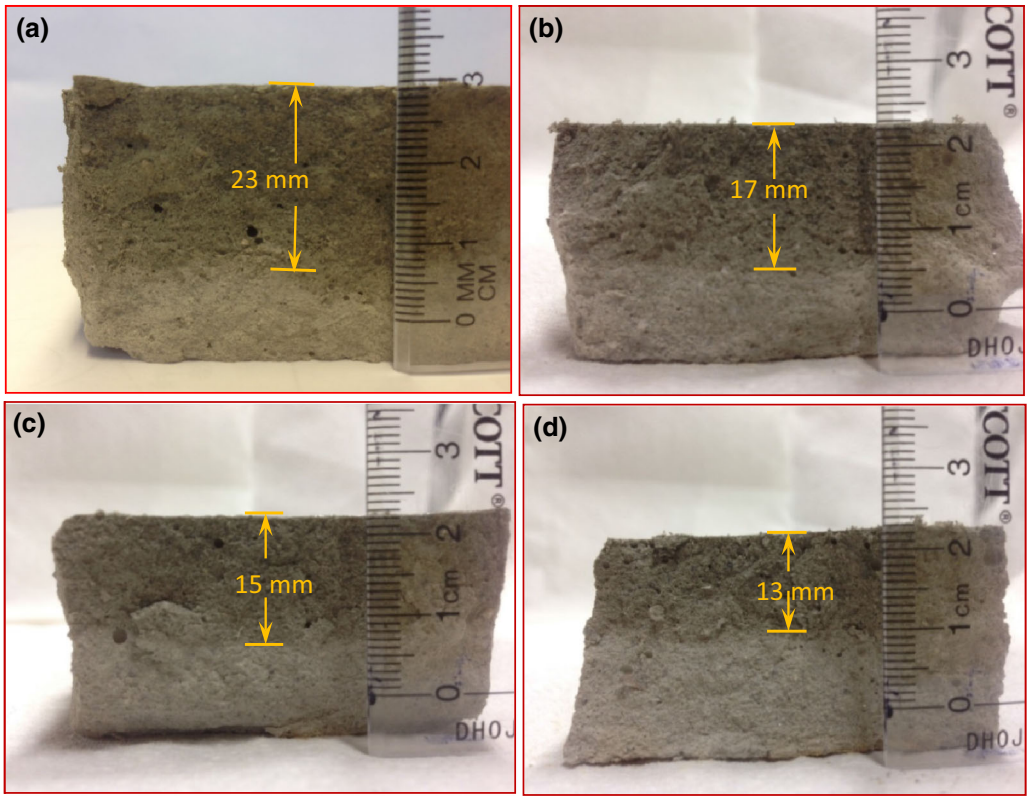


**Fig. 3** Typical pictures showing infiltration depth of biopolymer solution into dry MT 30 min after spraying: **a** 0 % (water only), **b** 0.3 %, **c** 0.5 %, and **d** 0.8 % concentrations

is because of the generation, propagation, and interaction of multiple cracks during penetration.

The average, standard deviation (SD), and coefficient of variation (COV) of the ten measured maximum penetration forces for each biopolymer concentration are summarized in Table 1, and the average of measured maximum penetration forces from the two first penetration tests for each biopolymer concentration is shown in Fig. 6. One can clearly see that the surface strength of MT increases with higher biopolymer concentration. The increase in the surface strength of MT can be attributed to the coating and binding of MT particles by the cross-linking biopolymer network. Xanthan gum is an anionic polysaccharide with a long-chain structure containing numerous hydroxyl groups, enabling it to form ionic bonds and hydrogen bonds with MT particles, causing a high degree of aggregation at the surface of MT [7]. Also, the cross-linking biopolymer network can bind detached particles and fill the voids between them, leading to formation of a denser structure and hence higher surface strength. The surface strength reflects the bonding strength between the MT particles and the amount of energy required to break down the crust [28]. A stronger crusted surface means more energy required from the saltation impacts to release the fine particles (dust) and thus higher resistance to wind erosion.

## 5 Numerical simulations

The experimental study indicates that biopolymer treatment can effectively increase the surface strength of MT. To better understand biopolymer stabilization of MT, DEM simulations were performed to simulate the first penetration test (P1) on MT specimens treated with biopolymer solutions of different concentrations.

### 5.1 Model description

The DEM simulations were performed using PFC3D v4.0. The bonding between MT particles was simulated using the default parallel bond model provided in the PFC3D [27]. Figure 7 shows the numerical model used in the DEM simulations. The flat-ended penetrometer with a diameter of $d = 6$ mm, the same size as that used in the physical experiments, was simulated using two walls—a horizontal disk wall and a vertical sleeve wall. Since the penetration depth is only 4 mm, the resistance derived from the sleeve wall of the penetrometer is expected to be very small and negligible. So it is assumed that the sleeve wall is frictionless and the flat end is frictional with a friction coefficient of 0.45 between it and the MT particles. The cylindrical box containing MT particles has a height of

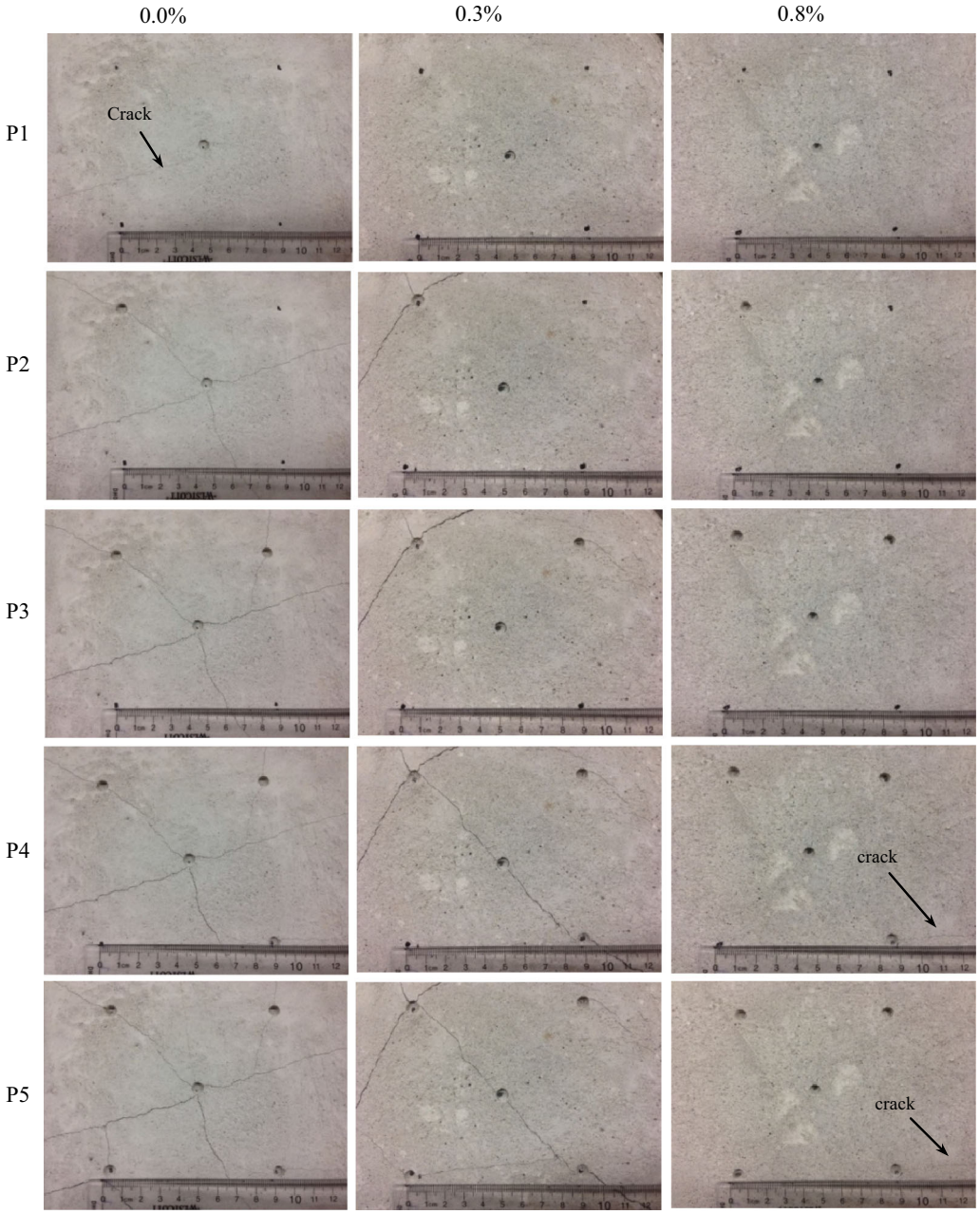


**Fig. 4** Comparison of surface conditions after each penetration test on MT specimens treated with biopolymer solution at a concentration of 0, 0.3, and 0.8 %, respectively

$H = 60$ mm and a diameter of $D = 120$ mm. A friction coefficient of 0.45 was assumed between the wall of the box and the MT particles. The normal and shear stiffnesses were set as $1 \times 10^9$ N/m for all walls. The simulated MT specimens were divided into two layers: the top-crusted layer with biopolymer stabilization and the bottom layer with no biopolymer stabilization. The thickness of the top-crusted layer ($h$) was set as 24, 17.5, 15, and 13 mm for the MT specimens treated with biopolymer solution at a concentration of 0, 0.3, 0.5, and 0.8 %, respectively, based on the measured infiltration depth at each condition in the previous section. The MT particles were represented by balls with diameters following a uniform distribution from 0.5 to 1.0 mm for the top layer and 0.8 to 1.6 mm for the bottom layer, respectively. Larger particle size was used for the bottom layer aiming to reduce the total number of particles and thus the calculation time.

The expansion method was adopted to generate the particle assembly with a target porosity of 0.35 for both the top and bottom layers. After generation of all particles,

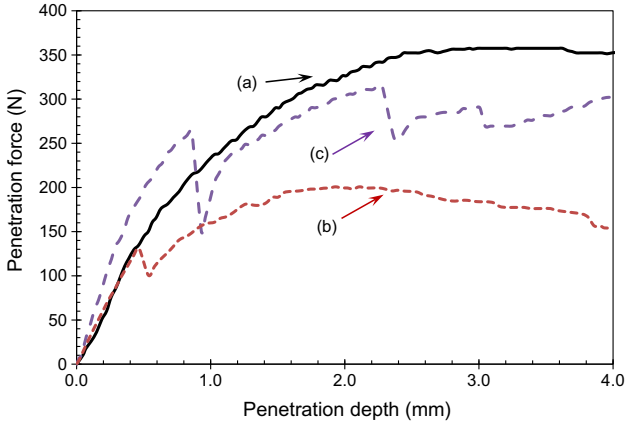


**Fig. 5** Typical penetration force versus penetration depth curves from penetration tests: (*a*) the penetration force increases steadily with penetration depth with no drop; (*b*) one obvious drop during the penetration; and (*c*) multiple drops during the penetration

**Table 1** Average, standard deviation (SD), and coefficients of variation (COV) of measured maximum penetration forces for MT specimens treated with biopolymer solutions of different concentrations

| Concentration (%) | Average (*N*) | SD (*N*) | COV (%) |
|---|---|---|---|
| 0.0 | 213.8 | 62.0 | 29.0 |
| 0.3 | 278.4 | 58.9 | 20.8 |
| 0.5 | 312.5 | 82.4 | 26.4 |
| 0.8 | 331.8 | 65.9 | 19.9 |

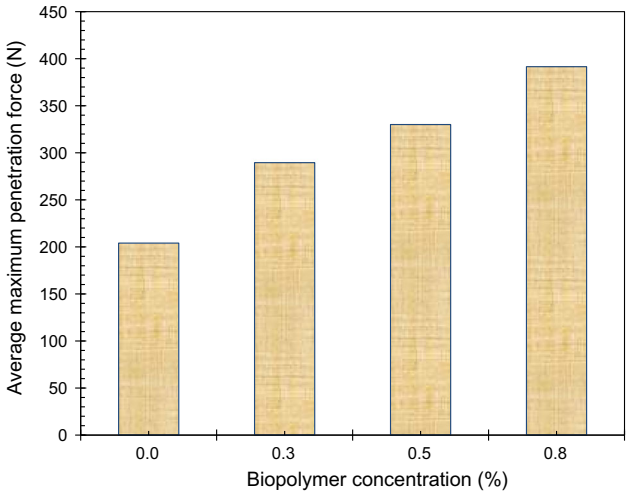


**Fig. 6** Average maximum penetration force of the two first penetration tests on MT specimens treated with biopolymer solution at a concentration of 0, 0.3, 0.5, and 0.8 %, respectively

different micro-properties were assigned to the top and bottom layers. All the MT particles were assigned the same density of 2650 kg/m$^3$. The flat-ended penetrometer was set at 2 mm above the surface of the specimen before

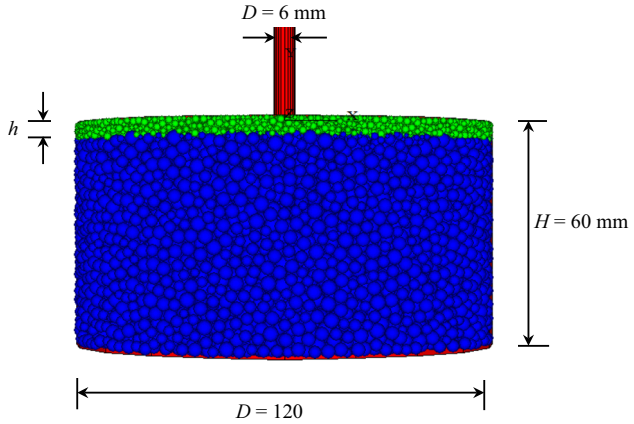


**Fig. 7** Numerical model of penetration test

**Table 2** Micro-parameters used in DEM simulations

| Micro-parameters | Description |
|---|---|
| *Particle* | |
| $k_n$ | Normal stiffness of the particle |
| $k_s$ | Shear stiffness of the particle |
| $\mu$ | Particle friction coefficient |
| *Parallel bond* | |
| $\overline{k}_n$ | Normal stiffness of the parallel bond |
| $\overline{k}_s$ | Shear stiffness of the parallel bond |
| $\overline{\lambda}$ | Radius multiplier |
| $\overline{\sigma}_c$ | Tensile strength of the parallel bond |
| $\overline{\tau}_c$ | Shear strength of the parallel bond |

testing. And then the top wall of the box was deleted, and the penetrometer was driven at a vertical velocity of 4 mm/s up to a penetration depth of 4 mm. The time step used was $2 \times 10^{-5}$ s. The tip resistance of the penetrometer and the number of cracks were recorded during the penetration process.

### 5.2 Calibration of micro-parameters

The micro-parameters used in the DEM simulations are listed in Table 2. To reduce the effort of calibration, some of the micro-parameters that only have minor effect on the mechanical response of the simulated material were predetermined based on experience and the information from the literature: $k_n/k_s = 1$, $\overline{\lambda} = 1$ and $\overline{k}_n/\overline{k}_s = 2$.

It is assumed that the elastic moduli of the parallel bond and the particle ($\overline{E}_c$, $E_c$) are equal to each other [27]. So the normal stiffnesses of the parallel bond ($\overline{k}_n$) and the particles ($k_n$) can be calculated using the following equations [27]:

$$k_n = 4RE_c \quad (1)$$

$$\overline{k}_n = \overline{E}_c/(R_A + R_B) \quad (2)$$

where $R$ is particle radius, and $A$ and $B$ represent two adjacent particles A and B. The normal stiffnesses of the parallel bond and the particles were calibrated to match the Young's modulus.

**Table 3** Calibrated micro-parameters for MT treated with biopolymer solutions of different concentrations

| Top layer/concentration | Micro-parameter | Value |
|---|---|---|
| 0.0 % | $\mu$ | 0.40 |
| | $\overline{\sigma}_c$ | 2.5 MPa |
| | $\overline{\tau}_c$ | 1.25 MPa |
| | $k_n = k_s$ | 0.12 MN/m |
| | $\overline{k}_n = 2\overline{k}_s$ | 26 GPa/m |
| 0.3 % | $\mu$ | 0.45 |
| | $\overline{\sigma}_c$ | 3.0 MPa |
| | $\overline{\tau}_c$ | 1.40 MPa |
| | $k_n = k_s$ | 0.15 MN/m |
| | $\overline{k}_n = 2\overline{k}_s$ | 30 GPa/m |
| 0.5 % | $\mu$ | 0.50 |
| | $\overline{\sigma}_c$ | 3.6 MPa |
| | $\overline{\tau}_c$ | 1.6 MPa |
| | $k_n = k_s$ | 0.17 MN/m |
| | $\overline{k}_n = 2\overline{k}_s$ | 36 GPa/m |
| 0.8 % | $\mu$ | 0.55 |
| | $\overline{\sigma}_c$ | 4.0 MPa |
| | $\overline{\tau}_c$ | 2.0 MPa |
| | $k_n = k_s$ | 0.216 MN/m |
| | $\overline{k}_n = 2\overline{k}_s$ | 48 GPa/m |
| Bottom layer | All micro-parameters are the same as those at 0.0 % concentration | |

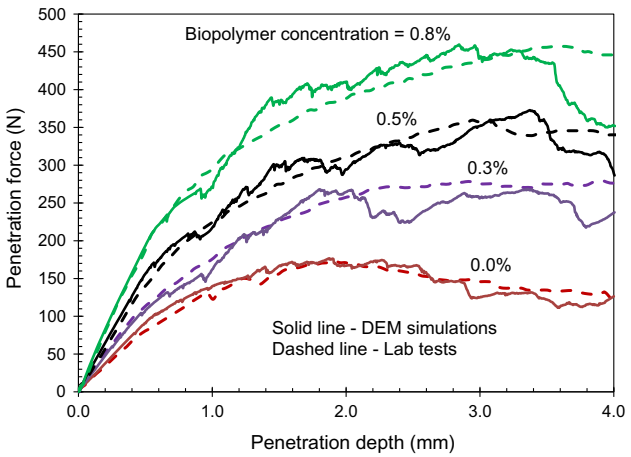


**Fig. 8** Comparison of penetration force versus penetration depth curves obtained from DEM simulations and laboratory tests on MT specimens treated with 0, 0.3 0.5, and 0.8 % biopolymer solutions, respectively

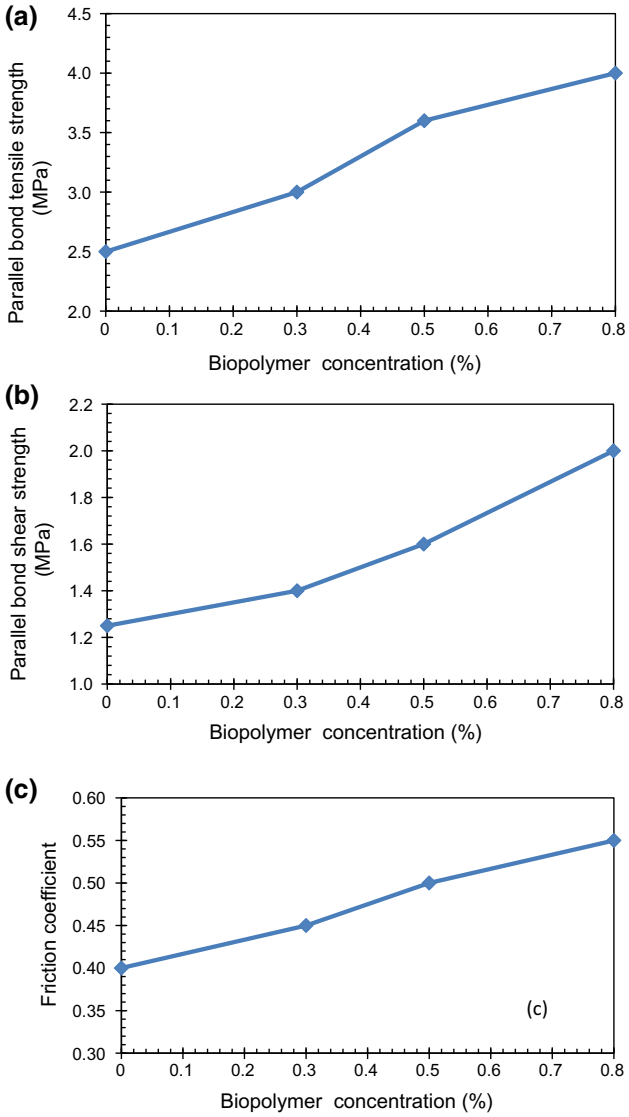


**Fig. 9** Effect of biopolymer concentration on **a** the parallel bond tensile strength, **b** the parallel bond shear strength, and **c** the particle friction coefficient, used in DEM simulations

The friction coefficient $\mu$ and the parallel bond strengths ($\overline{\sigma}_c$, $\overline{\tau}_c$) were calibrated to match the peak force obtained from the penetration test. The calibration was carried out by trial and error to adjust the input micro-parameters so that the simulation results match the experimental results. First, the micro-parameters were calibrated to match the penetration force–penetration depth response of the MT specimen treated with only water. Then, the obtained micro-parameters were assigned to the particles in the bottom layer, and the micro-parameters for the particles in the top layer were further calibrated to match the penetration force–penetration depth responses of the MT treated with biopolymer solution at a concentration of 0.3, 0.5, and 0.8 %, respectively.

## 6 Results of numerical simulations

Table 3 summarizes the micro-parameters used in the PFC3D simulations to reproduce the penetration force–penetration depth curves from physical experiments. Figure 8 shows the comparison of penetration force–penetration depth curves from DEM simulations with those from experiments for MT treated with 0, 0.3, 0.5, and 0.8 % biopolymer solutions, respectively. It can be seen that the DEM simulations can capture the force–penetration response of the tested MT specimens very well.

Figure 9 presents the obtained $\overline{\sigma}_c$, $\overline{\tau}_c$ and $\mu$ values from DEM simulations for MT treated with biopolymer solutions of different concentrations. Figure 9a, b shows that the parallel bond tensile and shear strengths both increase with higher biopolymer concentration, indicating that more biopolymer induces larger inter-particle bonding. This is beneficial to the enhancement of dust resistance because more energy is required to break the stronger bonding. Figure 9c shows that the inter-particle friction coefficient also increases with higher biopolymer concentration, which may be attributed to the aggregation of MT particles due to the presence of biopolymer.

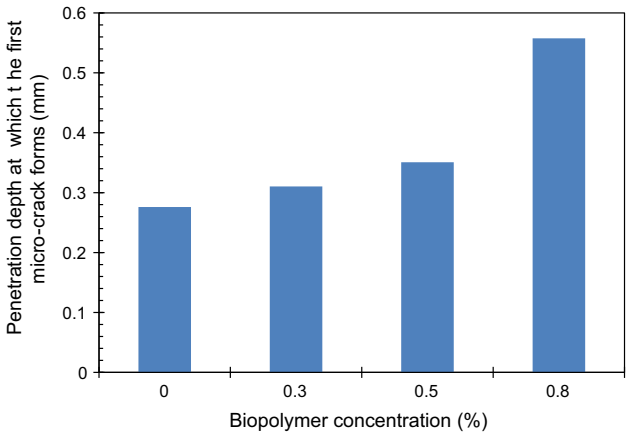


**Fig. 10** Effect of biopolymer concentration on the penetration depths when the first micro-crack forms during penetration

Figure 10 shows the effect of biopolymer concentration on the penetration depth when the first micro-crack forms during the simulated penetration test. With the increase in biopolymer concentration, simulated by increasing the inter-particle bonding, larger penetration depth is required for the formation of the first micro-crack. This indirectly confirms the experimental results shown in Fig. 4, which indicates that crack develops on the water-treated MT but not on the biopolymer-treated MT during the first penetration.

Figure 11 shows the contact force chains within the top 2 cm of the middle section slices of 10 mm thickness of the different numerical specimens at a penetration depth of 4 mm. The thickness of the lines represents the magnitude of the contact forces. A non-uniform distribution of the contact forces can be clearly seen. The contact force concentrates at the base of the penetrometer and branches out in a tree-like pattern to the base of the specimen. The maximum contact forces are 37.0, 54.6, 60.3, and 83.9 N

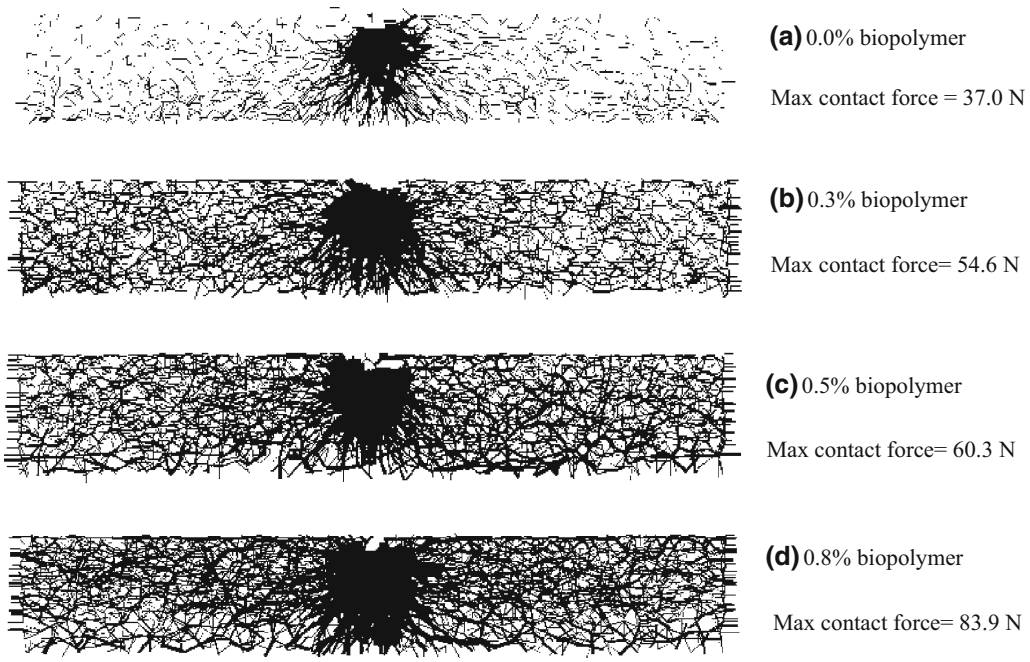


**Fig. 11** Contact force chains and maximum contact force within simulated MT treated with **a** 0 %, **b** 0.3 %, **c** 0.5 %, and **d** 0.8 % biopolymer solutions, respectively, at a penetration depth of 4 mm

for the MT specimens treated with 0, 0.3, 0.5, and 0.8 % biopolymer solutions, respectively. Higher biopolymer concentration leads to stronger bonding between MT particles and thus larger contact force that can be tolerated within the specimen and greater macroscale maximum penetration force.

## 7 Conclusions

The following conclusions can be drawn based on the experimental and numerical investigations of the surface strength of MT after biopolymer treatment:

a. The infiltration depth of biopolymer solution into dry MT decreases with higher biopolymer concentration. The infiltration depth of xanthan gum solution at a concentration of 0.8 % into dry MT is still large enough for effective crust formation and dust resistance enhancement.
b. Biopolymer stabilization effectively increases the surface strength and thus the dust resistance of MT, higher biopolymer concentration leading to greater increase.
c. The first penetration generates cracks on the water-treated MT specimen but not on the biopolymer-treated MT specimens. With increasing number of penetrations, more new cracks and crack coalescences are observed on the water-treated MT specimen than on the biopolymer-treated specimens, suggesting that biopolymer stabilization effectively increases the cracking resistance (related to tensile strength and thus dust resistance) of MT.
d. The DEM simulations using the parallel bond model can satisfactorily capture the measured penetration force versus penetration depth curves of MT treated with biopolymer solutions of different concentrations. The DEM simulations show that the parallel bond tensile and shear strengths both increase with higher biopolymer concentration, indicating that more biopolymer induces larger inter-particle bonding and thus increases the dust resistance of MT.

## References


1. Arroyo M, Butlanska J, Gens A, Calvetti F, Jamiolkowski M (2010) Cone penetration tests in a virtual calibration chamber. Géotechnique 61(6):525–531. doi:10.1680/geot.9.P.067
2. ASTM (2006) Standard classification of soils for engineering purposes. D2487-06, West Conshohocken, PA
3. Bea SA, Ayora C, Carrera J, Saaltink MW, Dold B (2010) Geochemical and environmental controls on the genesis of soluble efflorescent salts in Coastal Mine Tailings Deposits: a discussion based on reactive transport modeling. J Contam Hydrol 111(1–4):65–82. doi:10.1016/j.jconhyd.2009.12.005
4. Blight GE (2008) Wind erosion of waste impoundments in arid climates and mitigation of dust pollution. Waste Manag Res 26(6):523–533. doi:10.1177/0734242x07082027
5. Bolander P, Yamada A (1999) Dust palliative selection and application guide. Project Report 9977-1207-SDTDC, USDA San Dimas Technology and Development Center, San Dimas, CA
6. Butlanska J, Arroyo M, Gens A, O'Sullivan C (2013) Multi-scale analysis of cone penetration test (CPT) in a virtual calibration chamber. Can Geotech J 51(1):51–66. doi:10.1139/cgj-2012-0476
7. Chen R, Zhang L, Budhu M (2013) Biopolymer stabilization of mine tailings. J Geotech Geoenviron Eng 139(10):1802–1807. doi:10.1061/(asce)gt.1943-5606.0000902
8. Chen R, Lee I, Zhang L (2015) Biopolymer stabilization of mine tailings for dust control. J Geotech Geoenviron Eng 141(2): 04014100–04014110. doi:10.1061/(ASCE)GT.1943-5606.0001240
9. Chepil W, Woodruff N (1963) The physics of wind erosion and its control. Adv Agron 15:211–302
10. Copeland CR, Eisele TC, Chesney DJ, Kawatra SK (2008) Factors influencing dust suppressant effectiveness. Miner Metall Process J 25(4):215–222
11. Cundall PA (2001) A discontinuous future for numerical modelling in geomechanics? Proc ICE-Geotech Eng 149(1):41–47
12. Fuller J, Marsden L (2004) Practical dust control agent and application for alkaline ponds and playas. SME Annu Meet Prepr 2004:557–590
13. Gillette DA (1977) Fine particulate emissions due to wind erosion. Trans ASAE (Am Soc Agric Eng) 20:890–897
14. Gillette DA, Adams J, Muhs D, Kihl R (1982) Threshold friction velocities and rupture moduli for crusted desert soils for the input of soil particles into the air. J Geophys Res Oceans 87(C11): 9003–9015. doi:10.1029/JC087iC11p09003
15. Huang A-B, Ma MY (1994) An analytical study of cone penetration tests in granular material. Can Geotech J 31(1):91–103. doi:10.1139/t94-010
16. Jiang MJ, Yu HS, Harris D (2006) Discrete element modelling of deep penetration in granular soils. Int J Numer Anal Methods Geomech 30(4):335–361. doi:10.1002/nag.473
17. Karimi S (1998) A study of geotechnical applications of biopolymer treated soils with an emphasis on silt. PhD dissertation, University of Southern California, Los Angeles, CA
18. Kavouras IG, Etyemezian V, Nikolich G, Gillies J, Sweeney M, Young M, Shafer D (2009) A new technique for characterizing the efficacy of fugitive dust suppressants. J Air Waste Manag Assoc 59(5):603–612. doi:10.3155/1047-3289.59.5.603
19. Kim D, Quinlan M, Yen TF (2009) Encapsulation of lead from hazardous CRT glass wastes using biopolymer cross-linked concrete systems. Waste Manag (Oxf) 29(1):321–328. doi:10.1016/j.wasman.2008.01.022
20. Langston G, McKenna Neuman C (2005) An experimental study on the susceptibility of crusted surfaces to wind erosion: a comparison of the strength properties of biotic and salt crusts. Geomorphology 72(1–4):40–53. doi:10.1016/j.geomorph.2005.05.003
21. Lin J, Wu W (2012) Numerical study of miniature penetrometer in granular material by discrete element method. Philos Mag 92(28–30):3474–3482. doi:10.1080/14786435.2012.706373
22. Lobo-Guerrero S, Vallejo LE (2005) DEM analysis of crushing around driven piles in granular materials. Géotechnique 55(8):617–623. doi:10.1680/geot.2005.55.8.617
23. Lobo-Guerrero S, Vallejo LE (2007) Influence of pile shape and pile interaction on the crushable behavior of granular materials around driven piles: DEM analyses. Granul Matter 9(3–4): 241–250. doi:10.1007/s10035-007-0037-3

24. Lu H, Shao Y (1999) A new model for dust emission by saltation bombardment. J Geophys Res Atmos 104(D14):16827–16842. doi:10.1029/1999jd900169
25. Mak J, Chen Y, Sadek MA (2012) Determining parameters of a discrete element model for soil–tool interaction. Soil Tillage Res 118:117–122. doi:10.1016/j.still.2011.10.019
26. O'Brien P, McKenna Neuman C (2012) A wind tunnel study of particle kinematics during crust rupture and erosion. Geomorphology 173–174:149–160. doi:10.1016/j.geomorph.2012.06.005
27. Potyondy DO, Cundall PA (2004) A bonded-particle model for rock. Int J Rock Mech Min Sci 41(8):1329–1364. doi:10.1016/j.ijrmms.2004.09.011
28. Rice MA, Willetts BB, McEwan IK (1996) Wind erosion of crusted soil sediments. Earth Surf Process Landf 21(3):279–293. doi:10.1002/(SICI)1096-9837(199603)21:3<279:aid-esp633>3.0.CO;2-A
29. Rice MA, Mullins CE, McEwan IK (1997) An analysis of soil crust strength in relation to potential abrasion by saltating particles. Earth Surf Process Landf 22(9):869–883. doi:10.1002/(SICI)1096-9837(199709)22:9<869:aid-esp785>3.0.co;2-p
30. Richards L (1953) Modulus of rupture as an index of crusting of soil. Soil Sci Soc Am J 17(4):321–323
31. Skidmore E, Powers D (1982) Dry soil-aggregate stability: energy-based index. Soil Sci Soc Am J 46(6):1274–1279
32. Steevens J, Suedel B, Gibson A, Kennedy A, Blackburn W, Splichal D, Pierce J (2007) Environmental evaluation of dust stabilizer products. Environmental Laboratory, U.S. Army Engineer Research and Development Center, Vicksburg, MS